

Tri-rutile Layered Niobium-Molybdates for all Solid-State Symmetric Supercapacitor

Vipin Kumar,^{§#*} Jingwei Chen,[§] Shaohui Li,[§] Sebastian Matz,[‡] Venkateswarlu Bhavanasi,[§] Kaushik Parida,[§] Katharina Al-Shamery[‡] and Pooi See Lee^{§*}

V. Kumar, S. Li, V. Bhavanasi, K. Parida, P. S. Lee*

[§]School of Materials Science and Engineering, 50 Nanyang Avenue, Nanyang Technological University, Singapore-639798

[#]Centre For Energy Studies, Indian Institute of Technology Delhi, New Delhi, 110016, Delhi, India

*E-mail: pslee@ntu.edu.sg, vkumar@ces.iitd.ac.in

S. Matz, K. Al-Shamery

[‡]Physical Chemistry 1, Institute for Chemistry, Carl von Ossietzky University of Oldenburg, 26129, Oldenburg, Germany

1. Experimental section

Synthesis of the parent material: All the chemicals were directly used as purchased without any further purification. In this study, LiNbMoO₆ powder was chosen as the parent material. In the typical synthesis procedure, the oxides of Mo (MoO₃, 99.9% purity), Nb (Nb₂O₅, 99.97%) and lithium carbonate (Li₂CO₃) were mixed together in equal stoichiometric ratios (1:1:1), and the solid-state reaction was conducted at 580 °C for 24 hours with one intermediate grinding followed by quenching of the product in air atmosphere.

Protonation of LiNbMoO₆ powder to form HNbMoO₆H₂O nanosheets: The proton exchange of LiNbMoO₆ was carried out as reported in the literature with slight modification.¹ In this procedure, 500 mg of parent material was dissolved in 50 ml of 2M HNO₃ at room temperature for 4 days. After the protonation reaction, the product was washed with copious amount of DI water and dried at 70 °C for 10 hours.

Dehydration of HNbMoO₆H₂O nanosheets to form HNbMoO₆ nanosheets: To render the formation of HNbMoO₆ nanosheets, the as-prepared HNbMoO₆H₂O nanosheets powder was annealed at 230 °C for 3 hours in air atmosphere, the annealing temperature was predicted by the TGA analysis, as shown in **Fig. S1**.

Materials Characterizations:

The crystallographic phases of the materials were investigated using X-ray diffractometry (Shimadzu XRD 6000, Cu-K_α radiation, λ = 1.54 Å; power-2 kW). The morphologies were evaluated by Field-emission scanning electron microscopy (FESEM, JEOL 7600F), Transmission-

electron microscopy (TEM, JEOL JEM 2010) and Atomic Force microscopy (NT-MDT). Thermogravimetric analysis (TGA) was done using TA instruments Q2950. Fourier Transformation Infrared (FTIR) Spectroscopy was carried out using a Perkin Elmer, model spectrum GX instrument. Atomic force microscopy (AFM) (NT MDT – NTegra) was used to evaluate the thickness of the nanosheets. The X-ray photoelectron spectroscopy (XPS) was performed with a Thermo Scientific ESCALAb 250Xi spectrometer, using monochromated 1486.6 eV Al-K_α radiation with a spot width of 500 μm and a flood gun for charge compensation. The base pressure of the XPS systems was in the range of 10⁻¹⁰ mbar. All the peaks were fitted using a Shirley background and Voigt line shapes (Lorentzian-Gaussian). Electrochemical tests were performed using an AutoLab PGSTAT 30 potentiostat.

Electrochemical characterizations:

Preparation of the working electrodes: The working electrodes were prepared by mixing 85 wt% active materials, 10 wt% carbon black, and 5 wt% polyvinylidene fluoride (PVDF) in 500 μl of N-methyl-2-pyrrolidone (NMP). The mixture was then stirred overnight and the slurry was loaded on the graphite paper (1 cm × 1 cm in area) and dried in air at 100 °C for 10 h.

Preparation of the hydrogel and redox-mediated hydrogel electrolyte: The PVA/H₂SO₄ polymer electrolyte and redox-mediated hydrogel electrolyte were prepared according to the procedure reported in the literature with slight modification in concentration. First, 2 g of PVA (HiMedia, MW = 70000–100000) was mixed with 20 mL of hot (80 °C) water with constant stirring for 5 h to form a clear solution. Then, 2 g of concentrated H₂SO₄ was added into the above solution followed by 10 ml of DI water. Subsequently, after 1 h, 0.5 g of Na₂MoO₄ was dissolved in 10 ml of DI water and drop wise added into the above solution with constant stirring, and it was kept until formation of a gel-like solution.

Electrochemical testing of the electrodes: Electrochemical testing of the samples was done using a PGSTAT 30 potentiostat. In a three electrodes cell configuration Ag/AgCl, Pt plate and as-prepared electrodes were used as reference electrode; counter electrode and working electrodes, respectively. A prototype symmetric device was configured using two physically equivalent electrodes (slurry on graphite paper) with a total mass of ~2.4 mg (excluding the mass of filter paper and electrolyte) separated using an Advantec filter paper. The symmetric supercapacitors are fabricated using liquid as well as gel electrolytes (with and without redox mediator), where, a

filter paper soaked in 1 M H₂SO₄ is used as ionic medium for aqueous supercapacitor, while, solid state supercapacitor devices utilized ~100 µl of gel electrolyte to conduct electrolyte ions. After that the electrodes were sandwiched together to form a prototypical symmetric device they were directly connected to the electric wires to measure the performance.

Capacitance calculation:

The capacitance of the device is calculated using following formula

Specific capacitance (C_{sp}) taking scan rate into account is calculated using following equation;

$$C_{sp} = Q_{sp}/V \text{ (Fg}^{-1}\text{)}$$

Where, C_{sp} and Q_{sp} shows specific capacitance and specific charge, respectively, V is the operating potential window.

Specific capacitance (C_{sp}) taking Galvanostatic charge/discharge into account is calculated using following equation;

$$C_{sp} = I \times t_d/V \text{ (Fg}^{-1}\text{)}$$

Where, I is the applied current density in Ag^{-1} , and t_d is the discharge time.

Volumetric capacitance (C_v) is calculated using following equation;

$$C_{sp} = I \times t_d/D \times V \text{ (Fcm}^{-3}\text{)}$$

Where, I is the applied current density in Acm^{-2} , and t_d is the discharge time, D is the thickness of the active material on the electrodes.

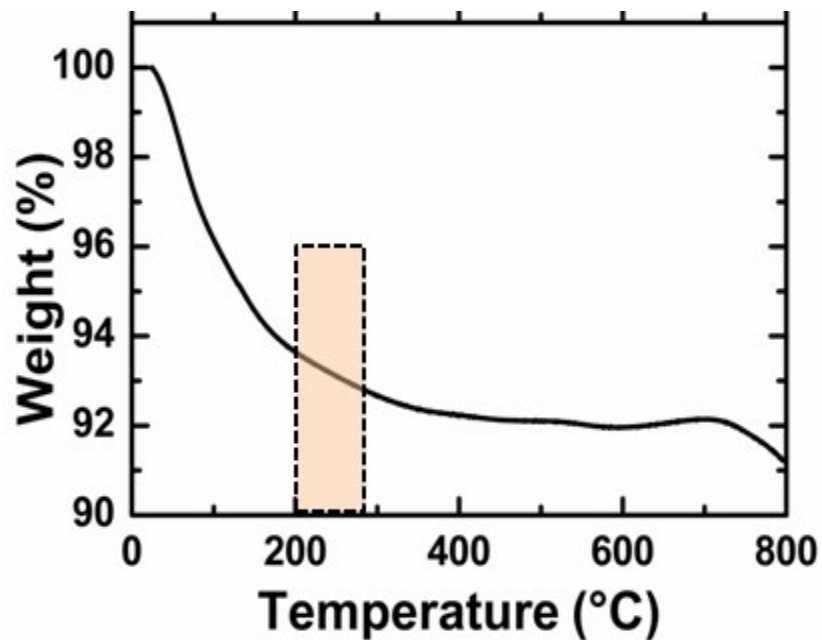


Fig. S1. Thermogravimetric analysis of $\text{HNbMoO}_6\text{H}_2\text{O}$

The shaded region in the mass vs. temperature curve indicates the range of temperature corresponding to removal of the water molecules.

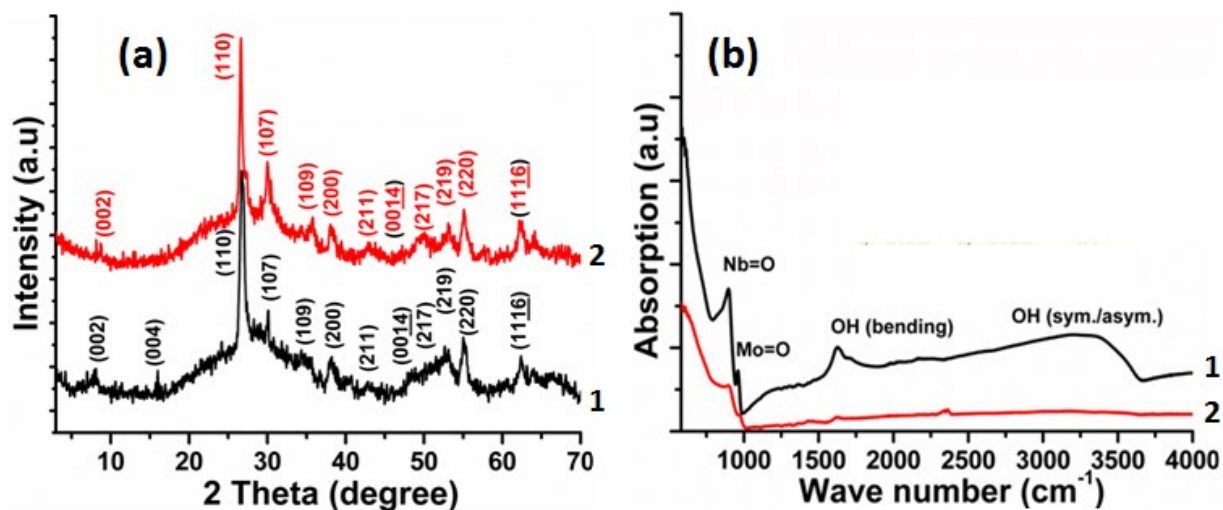


Fig. S2. XRD spectra of (a) $\text{HNbMoO}_6\text{H}_2\text{O}$ (1) and HNbMoO_6 (2) and (b) FTIR spectra of $\text{HNbMoO}_6\text{H}_2\text{O}$ (1) and HNbMoO_6 (2).

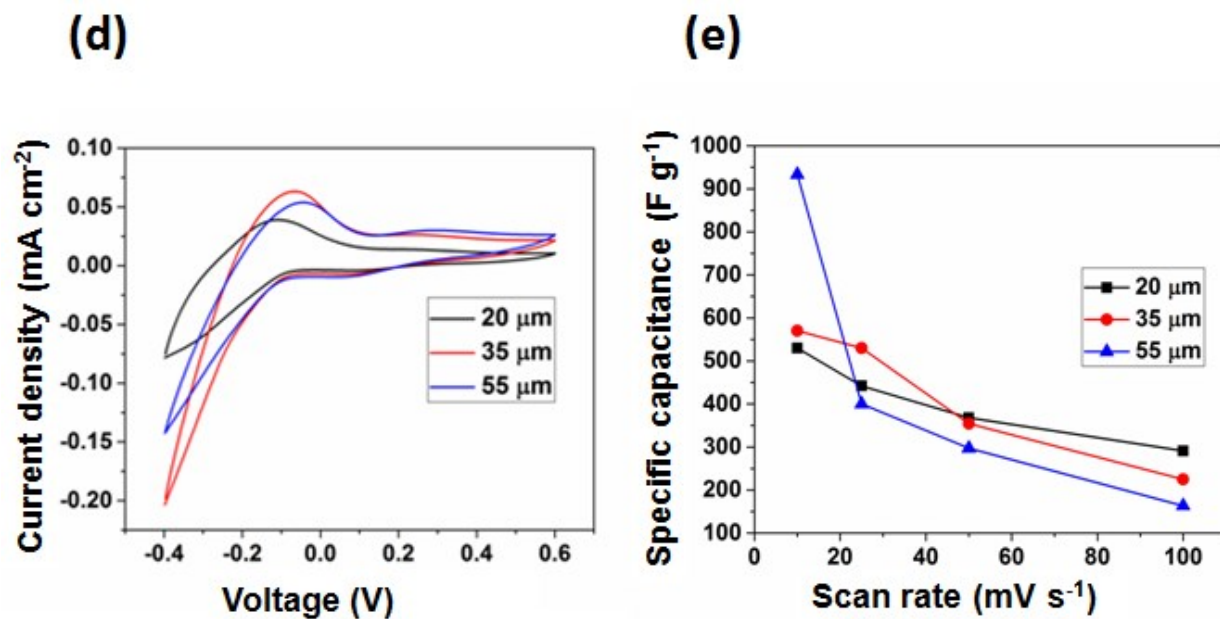
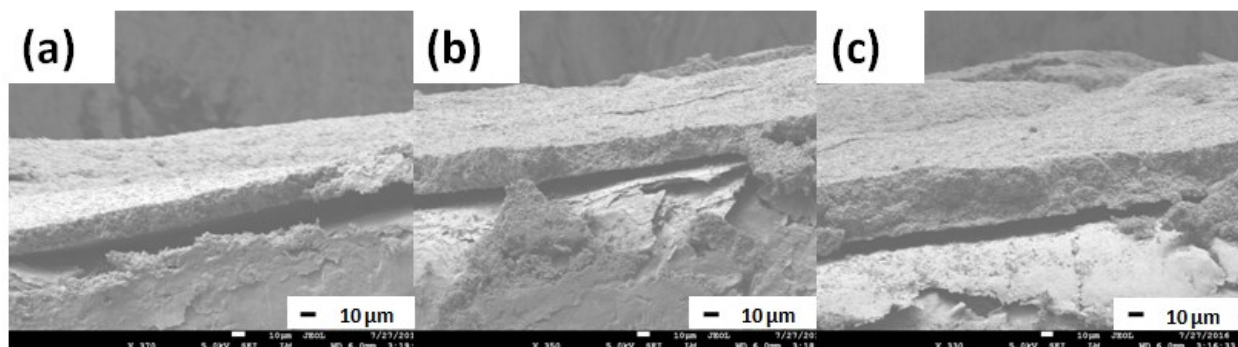


Fig. S3. (a-c) FESEM micrograph of various thicknesses of the HNbMoO₆ electrode. (d) CVs of HNbMoO₆ electrodes (various thicknesses) in H₂SO₄ electrolytes, and (e) specific capacitance as a function of scan rate.

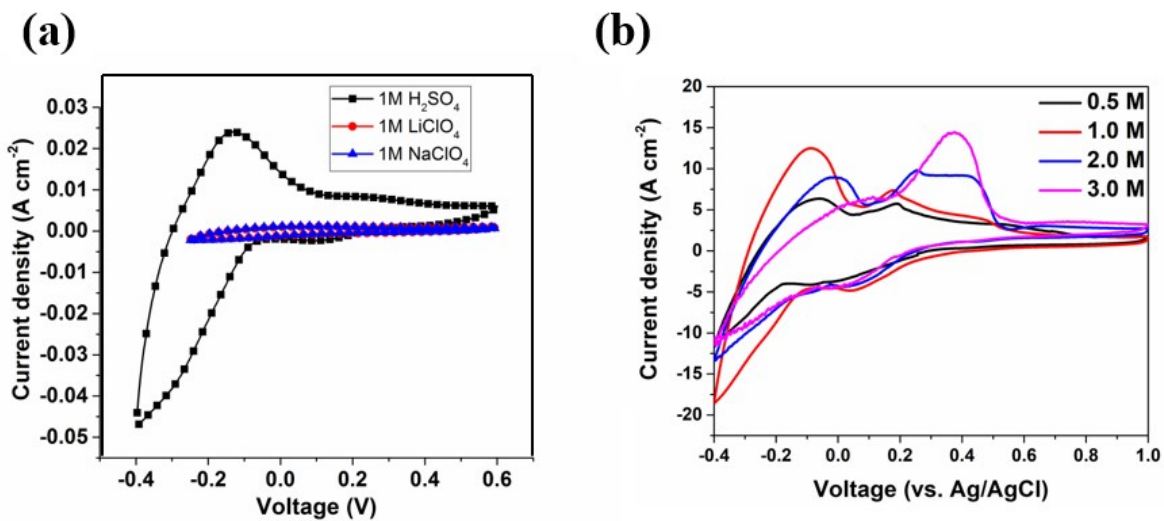


Fig. S4. (a) CVs of an HNbMoO₆ electrode in various electrolytes, and (b) Cyclic voltammograms (CV) of HNbMoO₆ electrodes recorded under various concentration of H₂SO₄.

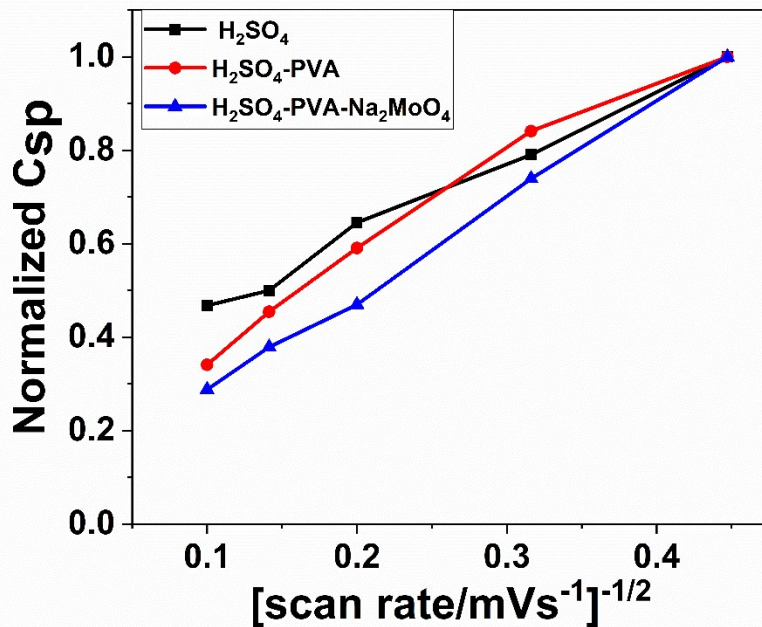


Fig. S5. Normalized C_{sp} vs (v)^{-1/2} allows separation between diffusion assisted and surface assisted charge storage reactions.

Table S1. Binding energies of the elements present in HNbMoO₆ electrode before and after charged and discharged states.

State	Mo3d _{3/2} / Mo3d _{5/2}	Nb3d _{3/2} / Nb3d _{5/2}	O1s			
Pristine	236.0 eV/ 232.9 eV	210.2 eV/ 207.5 eV				530.4 eV
Discharged	235.8 eV/ 232.4 eV	210.9 eV/ 208.2 eV	207.4 eV	533.8 eV	532.2 eV	530.8 eV
Charged	235.9 eV/ 232.8 eV	210.9 eV/ 208.1 eV	207.4 eV	533.6 eV	532.1 eV	530.7 eV

2. Modulation in the electrochemical potential window of HNbMoO₆

In the construction of the lattice in the layered HNbMoO₆, the lattice of MoO₃ and Nb₂O₅ partake mutually in the diffusion reactions, as explained in the experimental section. Electrochemical testing of HNbMoO₆, MoO₃ and Nb₂O₅ reveal that the potential window of the HNbMoO₆ electrode can be extended by the addition of Nb⁵⁺ ions (heterovalent cation substitution leaving one cationic vacancy behind), as shown in the Supporting information, **Fig. S8**. The origin of this intrinsic improvement in the electrochemical potential window lies in the molecular structure of H⁺Nb⁵⁺Mo⁶⁺O₆, as schematically illustrated in **Fig. S6**. Niobium in Nb₂O₅ exists in its highest oxidation state, i.e., Nb⁵⁺ with all the 4d electrons transferred to the 2p band of O, leaving the 4d band empty. On the other hand, the 4d band of MoO₃ is also empty, and exists as Mo⁶⁺. Here, we assume that the substitution of Mo⁶⁺ by Nb⁵⁺ ions results in the formation of cationic vacancies, which in response extends the reduction potential of the metal centers. In other words, due to the wide band gap nature of Nb₂O₅ (~3.4 eV),² the band of MoO₃ (~2.8 eV),³ can be well embedded into the band structure of Nb₂O₅, and provide additional surface charged-states (SS) near to the 4d band edge of Nb. The presence of these surface or bulk charged-states (SS) contributes to induce a dipolar-charge at the interface, leading to bending of the energy bands (Ev), thus, augmenting the energy barrier for the electrochemical reactions.

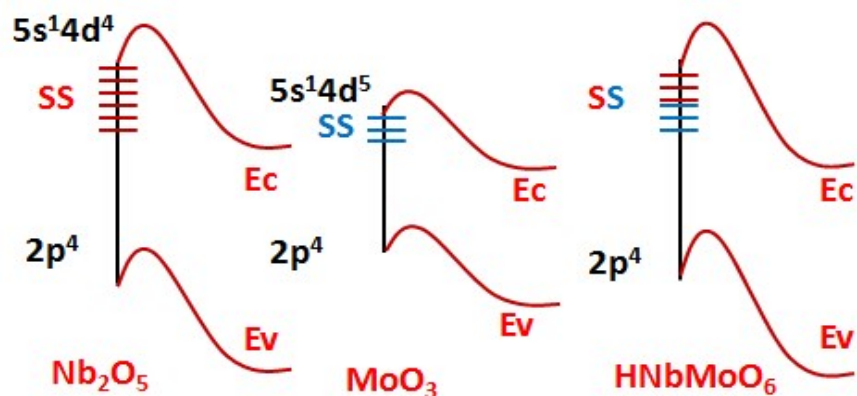


Fig. S6. Schematic of energy band structure of Nb_2O_5 , MoO_3 and HNbMoO_6 , Ec, Ev and SS are the conduction band edge, valence band edge and surface charged-states, respectively.

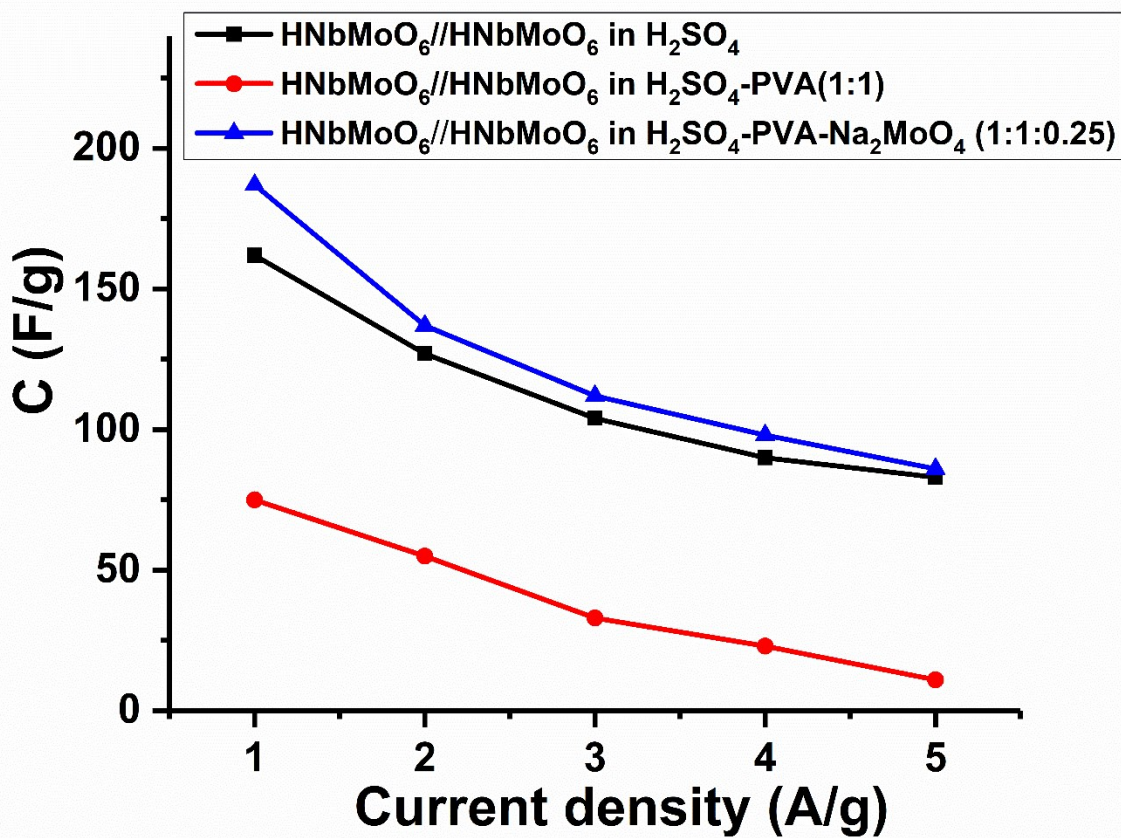


Fig. S7. Specific capacitance as a function of current density in various electrolytes.

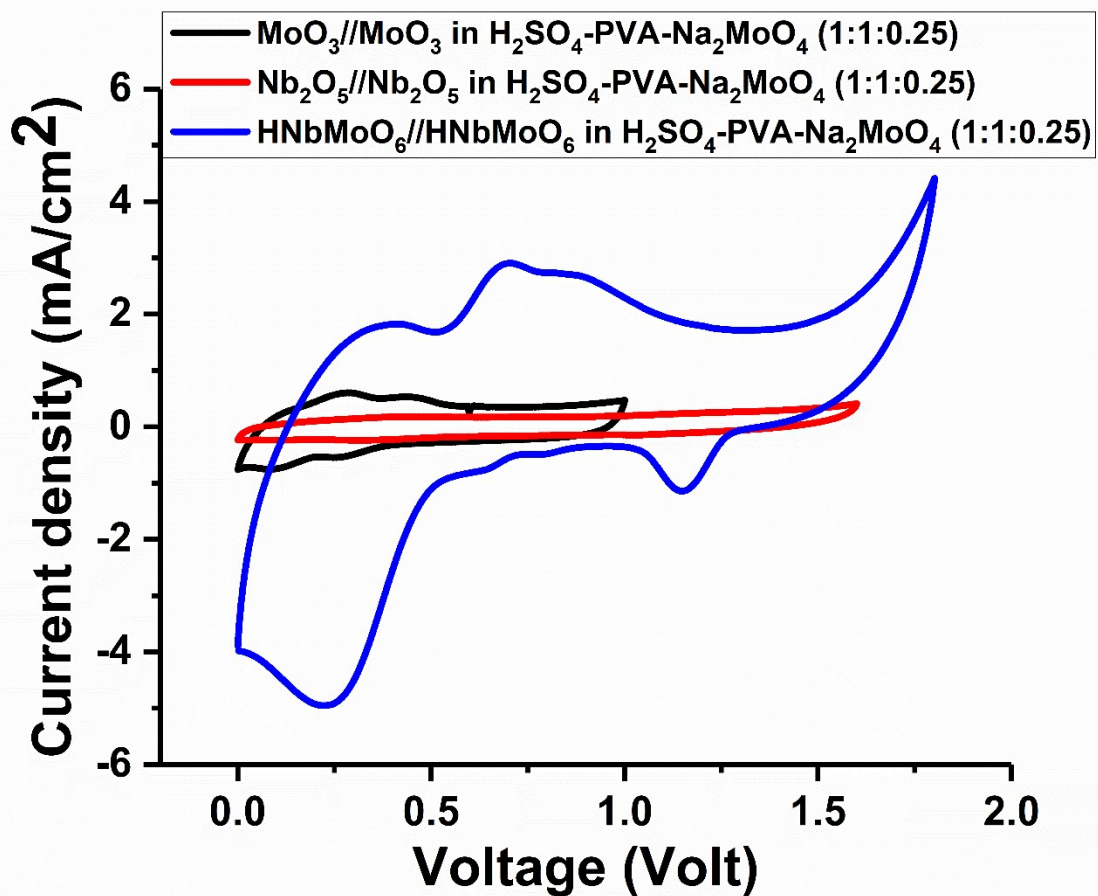


Fig. S8. CVs of a HNbMoO₆//HNbMoO₆, MoO₃//MoO₃ and Nb₂O₅//Nb₂O₅ solid state devices at a sweep rate of 25 mVs⁻¹, respectively.

Table S2. Comparison of the energy density and power density of various 2D material systems.

Electrode Materials	Energy density	Power density	Cycle number	Retention (%)	Ref.
MoS ₂ nanosheets/N-doped carbon	120 Wh kg ⁻¹	100 W kg ⁻¹	4000	85.5	<i>Small Methods</i> , 2019, 3 , 1900081 ²
MoS ₂ nanosheets	26 Wh kg ⁻¹	750 W kg ⁻¹	N/A	N/A	<i>ACS Appl. Mater. Interfaces</i> , 2019, 11 , 36991-37001 ³
CoS ₂	14.1 Wh kg ⁻¹	710 W kg ⁻¹	2000	92	<i>Mater. Res. Bull.</i> , 2019, 116 , 59 ⁴
Zn-Co-S nanosheets	85.1 Wh kg ⁻¹	460 W kg ⁻¹	6000	N/A	<i>Energy Storage Mater.</i> , 2020, 25 , 621-635 ⁵
MnO _x nanowires/Mo O _x nanosheets	23 Wh kg ⁻¹	2500 W kg ⁻¹	10000	90	<i>Small</i> , 2019, 15 , 1900862 ⁶
CoNi ₂ S ₄ nanosheets	67 Wh kg ⁻¹	800 W kg ⁻¹	10000	82	<i>Chem. Eng. J.</i> , 2019, 362 , 576–587 ⁷
HNbMoO₆ nanosheets	86 Wh kg⁻¹	900 W kg⁻¹	4000	63	This work

Reference

1. N. S. P. Bhuvanesh and J. Gopalakrishnan, *Inorg. Chem.*, 1995, **34**, 3760–3764.
2. J. Jiang, Y. Zhang, Y. An, L. Wu, Q. Zhu, H. Dou, and X. Zhang, *Small Methods*, 2019, **3**, 1900081.
3. S. G. Dalí, J. I. Paredes, J. M. Munuera, S. V. Rodil, A. Adawy, A. M. Alonso, and J. M. D. Tascoñ, *ACS Appl. Mater. Interfaces*, 2019, **11**, 36991-37001.
4. K. Lei, J. Ling, J. Zhou, H. Zou, W. Yang, S. Chen, *Mater. Res. Bull.*, 2019, **116**, 59–66.
5. F. Hekmat, H. Hosseini, S. Shahrokhian, U. H. Emrah, *Energy Storage Mater.*, 2020, **25**,

621-635.

6. Z. Ma, F. Jing, Y. Fan, L. Hou, L. Su, L. Fan, and G. Shao, *Small*, 2019, **15**, 1900862.
7. S. Rafai, C. Qiao, M. Naveed, Z. Wang, W. Younas, S. Khalid, C. Cao, *Chem. Eng. J.*, 2019, **362**, 576–587.